City-scale high-resolution flood models and the role of topographic data: a case study of Kathmandu, Nepal

C. Scott Watson, Januka Gyawali, Maggie Creed & John R. Elliott

View supplementary material ⧉

Published online: 10 Aug 2024.

Submit your article to this journal ⧉

Article views: 421

View related articles ⧉

View Crossmark data ⧉

Taylor & Francis
Taylor & Francis Group

City-scale high-resolution flood models and the role of topographic data: a case study of Kathmandu, Nepal

C. Scott Watson[a], Januka Gyawali[b], Maggie Creed[c] and John R. Elliott[a]

[a]COMET, School of Earth and Environment, University of Leeds, Leeds, UK; [b]Practical Action, Kathmandu, Nepal; [c]James Watt School of Engineering, The University of Glasgow, Glasgow, UK

ABSTRACT

Topographic data is a fundamental input to flood hazard models and controls the quality of the outputs. However, open-access global digital elevation models (DEMs) are dated and limited to 30 m resolution, which hinders modelling efforts in urban or topographically complex environments. We used the flood prone and expanding city of Kathmandu, Nepal, to evaluate the impact of topographic data source and resolution on flood model outputs. All DEMs evaluated featured spatially correlated topographic sinks with depths exceeding 20 m that required hydrological conditioning before being used in flood modelling. Incomplete hydrological conditioning appeared related to the overestimation of flood extent and therefore limited agreement when comparing a global 90 m resolution flood hazard model with a bespoke city-scale model at 10 m resolution (F1 score = 0.40). Instead, we found that the height above nearest drainage (HAND) metric was better able to replicate the higher resolution flood map as an indicator of flood susceptibility requiring only topographic information as an input. We also found that the computationally efficient FastFlood model was able to match the inundation extent (F1 score = 0.79) and flood depths (mean absolute error and root mean square error of 0.46 and 0.76 m respectively) of a published 10 m physics-based flood hazard model whilst requiring 212 times less computation time. Our analysis demonstrated that mapping city-scale flood inundation required hydrologically conditioned high-resolution topographic data but not physically complex flood models, highlighting the need for greater availability of high quality open access topographic data.

1. Introduction

An expanding and urbanising global population increases the intersection between people and natural hazards, including flooding, which is projected to increase with a warming

climate with more precipitation extremes (Min et al. 2011; Hoegh-Guldberg et al. 2018). Impacts are often greatest for the urban poor since land pressures promote informal development close to waterways (Pelling 1999; Reckien et al. 2017), often on floodplains (Di Baldassarre et al. 2013; Vollmer and Grêt-Regamey 2013).

Reducing flood risk requires combinations of risk sensitive planning (Mustafa et al. 2018; Jenkins et al. 2022) and adaptation strategies, such as using greenspaces and sustainable urban drainage systems to attenuate and store flood water (Kim et al. 2016; Webber and Samaras 2022), and taking source-to-sink approaches to catchment management (Wheater and Evans 2009; Hewett et al. 2020; Bourke et al. 2022). Flood risk changes in response to dynamic hydrological and river conditions, changing exposure of people and infrastructure, and changing climate (Merz et al. 2014). Additionally, flood hazard and risk maps are a function of different modelling approaches and input datasets, where topographic data is a critical input (Wechsler 2007; Neal et al. 2012; Yalcin 2020).

Quantifying flood hazard in an urban environment requires topographic data in the form of digital elevation models (DEMs) capable of representing the interaction of fluvial and pluvial flows with city infrastructure such as roads, buildings, and bridges. DEMs can be derived at ∼1.5 m resolution using commercial satellite imagery or sub-metre resolution from aerial photogrammetry and lidar surveys (Smith et al. 2015) (Figure 1). However, open access DEMs at the global scale are generally restricted to 30 m resolution, for example the Shuttle Radar Topography Mission (SRTM) DEM acquired in 2000 (Farr et al. 2007). Whilst flood models using 30 m resolution DEMs can produce useful outputs for large geographic areas (Wing et al. 2017; Bates et al. 2021), limitations related to the topographic resolution, accuracy, and date of acquisition are often greatest in built-up areas where robust information on flood hazard and risk is required (Sampson et al. 2016). Therefore, higher resolution DEMs are required to produce accurate flood models in urban environments (Fewtrell et al. 2008; Hawker et al. 2018; Xing et al. 2019), with coarser resolution DEMs producing greater uncertainties including overprediction of flood extents due to a lack of river channel definition (Saksena and Merwade 2015; Farooq et al. 2019; Xing et al. 2019; Muthusamy et al. 2021). Pre-processing using filling, carving, or a combination of the two approaches is also necessary to create a hydrologically conditioned DEM for hydraulic modelling or before applying DEM-based methods of delineating stream networks (Martz and Garbrecht 1992; Saunders 2000; Reuter et al. 2009) (Figure 1c).

High-resolution DEMs and the computation resource and expertise required to use them in city-scale flood models are not widely accessible, which may necessitate the use of coarser resolution models or simplified indicators of flood susceptibility. In some cases, simplified approximations of flood susceptibility may be more appropriate to identify potentially hazardous areas and therefore guide detailed physics-based hydraulic modelling studies, such as when planning for future urban development (Galasso et al. 2021; Jenkins et al. 2022). For example, multiple flood inundation scenarios that reflect spatially variable precipitation extents within a large catchment can be combined to inform flood hazard (Tufano et al. 2023). Alternatively, topographic indicators of potential flood inundation such as height above the nearest drainage (HAND) (Rennó et al. 2008; Nobre et al. 2011) require only a DEM but do not incorporate any probabilistic information on flood return period (McGrath et al. 2018; Rincón et al. 2018; Johnson et al. 2019).

In this study, we evaluate key issues surrounding the implications of DEM choice for flood modelling by evaluating published flood model outputs alongside those derived here. Specifically, we used topographic data spanning 10–90 m resolution, combined with derived flood hazard maps, to determine the impact of topography on hydrological
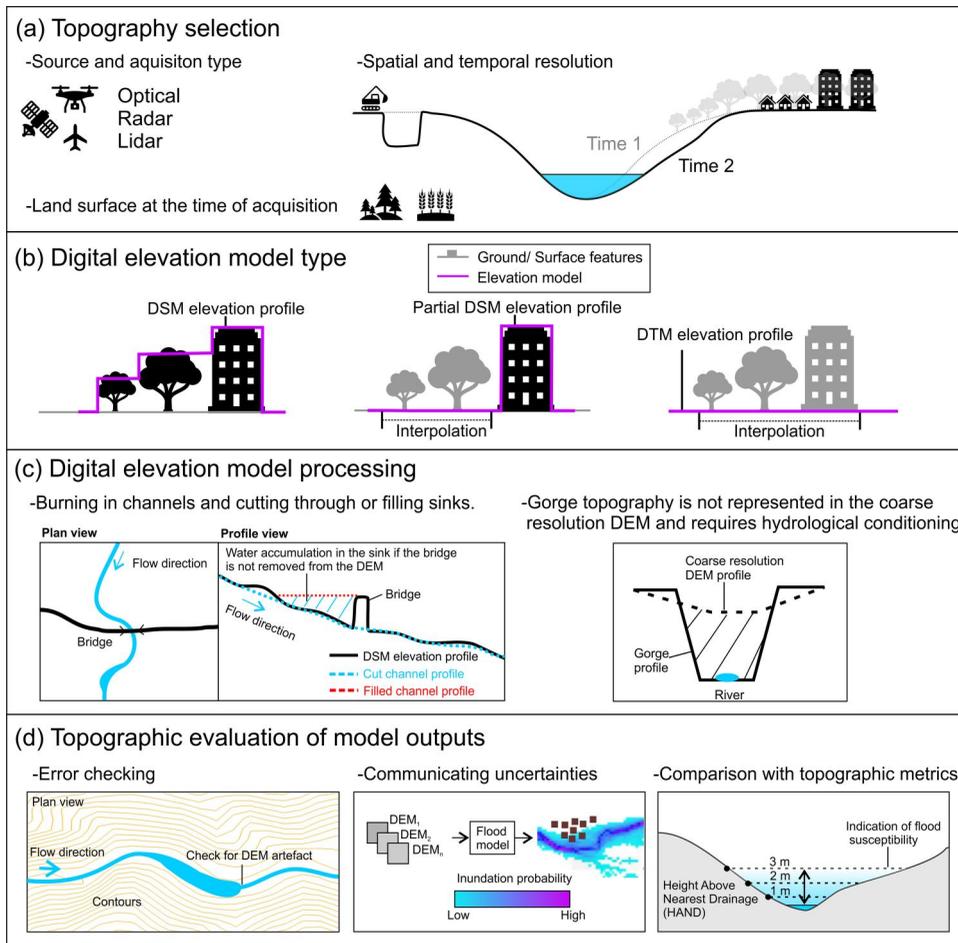
Figure 1. Topographic considerations for hydrological modelling. (a) Topographic data acquisition. The acquisition sensor and land surface characteristics affect the representation of features in the DEM. The land surface may also have changed between the DEM acquisition date and the time of study. (b) DEM type reflecting the inclusion (DSM) or exclusion (DTM) of surface features. (c) DEM processing for hydrological correction to remove anthropogenic features or correct for inadequate representation of the channel due to DEM resolution. (d) Evaluating model outputs with respect to topography, topographic uncertainties, and topographic indicators of flood susceptibility such as HAND.

outputs for the expanding and flood-prone city of Kathmandu, Nepal. Our objectives were to: (1) evaluate the quality of bespoke and global open access DEMs for representing stream networks and adjacent topography, (2) quantify differences with respect to flood extent outputs in published flood hazards maps and (3) evaluate the HAND and FastFlood models for deriving flood hazard information relevant to urban planning.

2. Methods

2.1. Study site

The Kathmandu valley features an urbanised centre surrounded by agricultural land and forested slopes and is primarily drained by the Bagmati River, which exits the watershed through steep topography in the southwest of the catchment (Figure 2). Built-up areas of
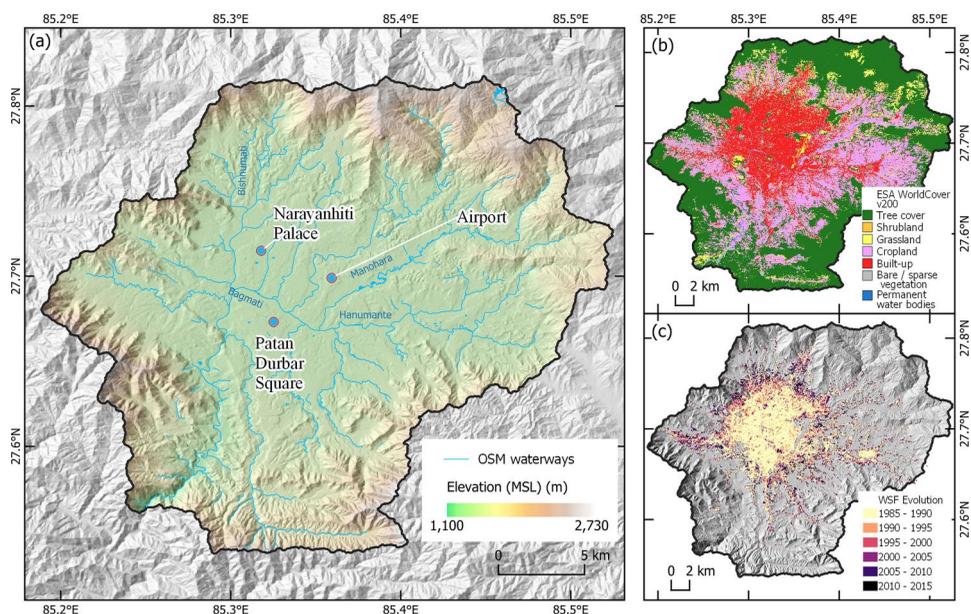
Figure 2. Overview of the study area covering the Kathmandu valley. (a) Catchment elevation from the copernicus 30 m DEM (Airbus Defence and Space GmbH 2020), (b) 2021 landcover classification from the ESA WorldCover v200 dataset (Zanaga et al. 2022), and (c) built-up area expansion 1985–2015 from the WSF evolution dataset (Marconcini et al. 2021).

the city are expanding due to urban migration, primarily on former agricultural land (Ishtiaque et al. 2017). More extreme precipitation events in combination with already overwhelmed drainage systems means flooding is a major and increasing issue in Kathmandu (Pradhan-Salike and Raj Pokharel 2017; Kc et al. 2021). Despite the requirement for flood hazard information, the only open access flood hazard maps that exist for Kathmandu are produced at 90 m resolution and are not recommended for 'detailed local scale assessments or engineering purposes' (METEOR Project Consortium 2019). This open source flood map and a higher resolution (10 m) flood hazard map that was recently published by Shrestha et al. (2023), will be evaluated in this study (section 2.4).

2.2. DEMs

We refer to DEMs as a general term for digital elevation models, including digital surface models (DSMs), which represent the elevation of the ground surface including buildings and vegetation, and digital terrain models (DTMs), which represent only the ground surface with surface features removed. A high-resolution DEM covering the 653 km² area of interest (AOI) (Figure 2) was created using tri-stereo Pleiades satellite imagery acquired in four acquisitions (27/10/2019, 18/12/2019, 25/12/2019, 13/01/2020). The panchromatic band (0.5 m resolution) was processed using rational polynomial coefficients (RPCs) to create a DSM with EGM2008 vertical referencing in Agisoft Metashape v1.8.4. All acquisitions were aligned in one bundle to produce a sparse point cloud, which was filtered to remove outliers using Metashape's gradual selection tools before producing a dense point cloud using *High* quality settings. The DEM was output at 1.5 m resolution and resampled to 10 m resolution for evaluation alongside the flood model outputs published by Shrestha et al. (2023), who also used this DEM.

Table 1. Summary of the DEMs used in this study.

DEM	Resolution	Acquisition period and source
Pleiades tri-stereo	10 m (downsampled)	27/10/2019–13/01/2020. Optical satellite imagery.
Copernicus 30 m resolution global DSM (GLO-30)	30 m	01/01/2011–07/01/2015. TanDEM-X radar mission.
Forest And Buildings removed Copernicus DEM (FABDEM)	30 m	01/01/2011–07/01/2015. TanDEM-X radar mission.
Multi-Error-Removed Improved-Terrain (MERIT)	90 m	February 2000. Shuttle Radar Topographic Mission (SRTM).

Selected open access DEMs were used for comparison with the high-resolution DEM (Table 1). The Copernicus 30 m resolution global DSM (GLO-30) was created from data acquired by the TANDEM-X mission (2011–2015) and represents the most recent and potentially best quality global DEM (Airbus Defence and Space GmbH 2020; Hawker et al. 2022). The Forest And Buildings removed Copernicus DEM (FABDEM) is a 30 m DTM created from the GLO-30 DSM by removing buildings and forests, which is designed to improve applicability for flood modelling (Hawker et al. 2022). Additionally, we used the 90 m Multi-Error-Removed Improved-Terrain (MERIT) DEM, which has forest height bias removed from the underlying SRTM DEM along with other artefact corrections (Yamazaki et al. 2017), in addition to the hydrologically conditioned version of MERIT called the MERIT Hydro (Yamazaki et al. 2019). The MERIT DEM was used to derive the published 90 m flood hazard products covering Kathmandu (METEOR Project Consortium 2019) (Section 2.3). All DEMs were coregistered to the GLO-30 DEM following the method of Nuth and Kääb (2011). The coregistration was performed using an estimate of the most stable ground areas by excluding *Tree cover* and *Permanent water bodies* classes from the ESA WorldCover v200 dataset (Zanaga et al. 2022) (Figure 2b). The normalised median absolute deviation (NMAD) was used to compare elevation differences between DEMs, since it is considered an estimate for the standard deviation less affected by outliers (Höhle and Höhle 2009; Shean et al. 2016).

2.3. Hydrological processing and stream networks

Topographic sinks were identified in each DEM using the *DepthInSink* tool of Whitebox 1.4.0 (Lindsay 2016). These sinks would accumulate water in a flood model until overtopped and therefore require pre-processing to mitigate. DEMs were hydrologically conditioned using the *BreachDepressionsLeastCost* tool using a search radius of 1–2 km, which breaches through sinks to permit downstream flow routing. Although breaching is generally preferable to 'fill' algorithms and creates more accurate stream networks (Lidberg et al. 2017), the breached river channel does not necessarily represent the true river thalweg. The breaching algorithm was selected for its ease of consistent application across each DEM, although more complex algorithms to preserve valid depressions whilst preserving flow direction have been developed (Jiang et al. 2023). We derived the stream and river channel network using D8 flow direction and a catchment flow accumulation threshold of 0.9 km^2 (1,000 cells for 30 m resolution DEMs). Therefore, the D8-derived inception of the stream network was consistent across DEMs and was selected to match the inundation output of Shrestha et al. (2023). These DEM-derived stream networks were compared with a manually digitised 64 km length of waterways, which was derived using high-resolution GoogleEarth basemap imagery dated 19th and 22nd November 2022. Here, the channel centreline was digitised at 1:1,000 scale with an estimated positional accuracy

of <5 m. OpenStreetMap Waterways were also downloaded for comparison with the reference stream network (OpenStreetMap Contributors 2022). Differences in the stream networks between DEMs would affect the positional accuracy of flood model outputs in respect to other datasets such as buildings and roads. Therefore, we analysed these offsets by measuring the horizontal distance between each DEM's stream network and the manually digitised reference stream network. The line vertices for each stream network were regularised at 5 m intervals and the closest point-to-point distance with the reference network was derived. Sinuosity was also derived for each stream reach defined as the stream length divided by the straight-line distance between the stream start and end (Nyberg et al. 2015).

2.3.1. KH-9 1974 satellite imagery

KeyHole-9 (Hexagon) satellite imagery from 1974 were used to evaluate longer-term changes in the stream network. Two stereo images from 23rd November 1974 (USGS EarthExplorer IDs: DZB1209-500101L007001 and DZB1209-500101L008001) were used to generate a DEM and orthorectified image in Agisoft Metashape v1.8.4 (e.g. Sevara 2013). The images were aligned using pre-calibrated camera parameters from Dehecq et al. (2020) and 15 ground control points (root mean square error = 9.90 m) were used for georeferencing using latitude and longitude information extracted from a Google Earth Basemap and elevation information from the GLO-30 DSM. The orthoimage was exported at 4 m resolution. The same extent of reference streams digitised in Google Earth was also manually digitised using the KH-9 satellite imagery.

2.4. Flood hazard maps

We used 90 m resolution flood hazard maps derived using the Fathom global flood hazard modelling framework (Sampson et al. 2015; Smith et al. 2015) on the MERIT DEM, which were published by the METEOR Project Consortium (2019). The outputs included pluvial and fluvial flooding for 1 in 5 (20% chance in any year) to 1 in 1,000 year (0.1% chance in any year) flood events, which were presented as floods depths in the range of 0–5 m. These maps were designed to provide regional scale information rather than data for local scale assessments (METEOR Project Consortium 2019); nonetheless, they represent the only open access flood hazard models covering Kathmandu. We also evaluated a 10 m resolution flood hazard map from Shrestha et al. (2023), which was produced using a 10 m DEM derived from the same Pleiades satellite imagery described in Section 2.2. This model was run using HAIL-CAESAR, which is a high performance version of the Caesar-Lisflood algorithm that uses a simplified version of the shallow water equations (Coulthard et al. 2013). The model was run using $2 \times$ AMD EPYC 7663 56-Core Processor working in hyperthreading housed in Edinburgh Parallel Computing Centre (EPCC) and took approximately 2.25 days to complete the run. We refer to this model throughout as the Shrestha et al. (2023) model.

We derived two flood hazard maps in this study using tools that can produce outputs in minutes to hours, compared to more complex flood models that would typically take days or weeks for single simulations at a city-scale. We first derived HAND maps from each hydrologically conditioned DEM using Whitebox's *ElevationAboveStreams* tool (Lindsay 2014). These maps show the relative elevation above the river channel on a pixel-by-pixel basis and therefore indicate flood susceptibility without considering the dynamics of flow routing. Like the other flood models in this study, the HAND elevations are relative to the river surface represented in the DEM without consideration of the

spatially variable river depth, which to account for would require cross section surveys. Second, we applied the FastFlood model (van den Bout et al. 2023) using rainfall for a 1 in 100 year median mid-future (2046–2075) flood event (246 mm of rainfall in 24 h). The magnitude of the rainfall was obtained from the non-stationary rainfall frequency analysis of Shrestha et al. (2023) Shrestha et al. (2023). In order to accurately compare the results of FastFlood and the flood maps in Shrestha et al. (2023) we used a Mannings value (0.03) and spatially variable rainfall as input to FastFlood (2023) and ran the solver with *Very High* accuracy and *Accounting for depressions* enabled. The FastFlood model uses an assumption of steady state flow that is compensated by using a flow network to estimate peak flow (van den Bout et al. 2023). The FastFlood model has shown good agreement with fully dynamic physics-based models with a 1,500 times reduction in computation time (van den Bout et al. 2023) and therefore is potentially well-suited to large scale high-resolution flood hazard modelling. We compared the HAND and FastFlood outputs with the published flood hazard maps described below.

When comparing flood model outputs, we take the physics-based Shrestha et al. (2023) model to be the reference and report accuracy metrics that describe how well the other models' outputs replicate this flood extent. For example, true positives indicate a modelled inundated area that is correctly predicted according to the reference dataset; false positives indicate the prediction of an inundated area that was incorrect; and false negatives indicate the presence of an inundated area that was not predicted by the model. We use the F1 score (1), which is a weighted average of precision (ratio of true positives to the total number of positive predictions) and recall (ratio of true positives to the total number of relevant instances) (e.g. Kabir et al. 2020). F1 score is a 0–1 scale where 1 is the highest accuracy. We also report the intersection over union (IoU) ratio (2), which quantifies the amount of overlap between the predicted flood extent and the reference flood extent of Shrestha et al. (2023). For these comparisons, we exclude small, isolated patches of flood inundation of ≤ 100 connected pixels (10,000 m^2).

$$F1 \; score = \frac{(\text{Precision} \times \text{Recall})}{(\text{Precision} + \text{Recall})/2} \tag{1}$$

$$IoU = \frac{\left(\begin{array}{c} Intersecting \; area \; of \; the \; predicted \; flood \; extent \\ and \; the \; reference \; flood \; extent \end{array}\right)}{\left(\begin{array}{c} Combined \; area \; of \; prediced \; flood \; extent \\ and \; the \; reference \; flood \; extent \end{array}\right)} \tag{2}$$

3. Results

3.1. DEM comparison

All results use the hydrologically corrected DEMs (2.3) other than for deriving DEMs of difference, where we compare the unmodified DEMs. The elevation differences between the GLO-30 and MERIT DEMs featured the largest normalised median absolute deviation (NMAD = 5.45 m), compared to the GLO-30 and FABDEM (4.05 m), and GLO-30 and Pleiades DSMs (1.82 m) (Figure 3). The GLO-30 and FABDEM difference showed a skewed distribution with a long tail of positive elevation differences, which are predominantly related to the subtraction of forest heights in the FABDEM (Figure 3b) to better approximate a bare-earth DTM (Hawker et al. 2022). Elevation differences between the GLO-30 and Pleiades DSMs were less pronounced and displayed spatial trends more aligned with real topographic changes (Figure 3c, Figure S1). Here, negative values
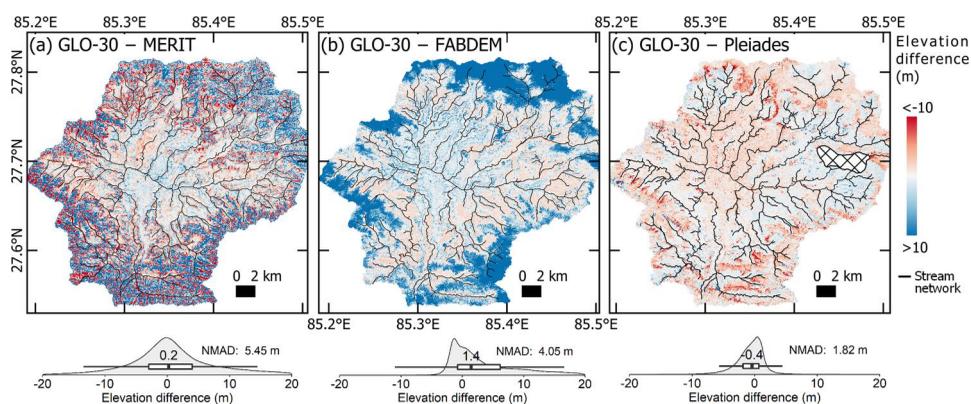
Figure 3. DEMs Of difference between the GLO-30 and the MERIT (a), FABDEM (b), and pleiades (c) DEMs. Rotated half violin plot below each panel shows the distribution of the elevation differences.

represent an elevation increase though time, since GLO-30 was produced with data collected 2011–2015, compared to 2019–2020 for the Pleiades DSM. Elevation decreases correspond with activities such as road construction and landslides (e.g. Figure S1a–c). In comparison, elevation increases are visible in the centre of the catchment over built-up areas corresponding to the construction of new buildings (e.g. Figure S1d), and also around the forested catchment edges.

All DEMs featured topographic sinks with depths exceeding 20 m at similar locations (Figure 4 – red markers). The Pleiades DSM sinks covered the smallest spatial extent 6% (40 km^2) of the catchment area (653 km^2), compared to 7% for the FABDEM, and 8% for the GLO-30 and MERIT DEMs. Sinks were located where the drainage network passed through topographic constrictions, such as Chobar Gorge (Figure 4a – label (1)), and these locations corresponded to areas of high depth in the coarse-resolution flood maps (Figure 4e).

3.2. River channel networks

The OSM and Pleiades DEM-derived stream networks showed closest agreement with the manually digitised reference stream network, with median horizontal differences of 4 m and 6 m, respectively (Figure 5a,b,h). The MERIT (year 2000 DEM) stream network had the largest horizontal difference compared to the reference streams with a median offset distance of 45 m. By comparison, 1974 KH-9 imagery revealed that the median horizontal change in the stream network 1974–2022 was 14 m, with most change occurring on the Manohara River in the east of the catchment (Figure 5g). Therefore, the change in the river course over this 48-year period was localised (e.g. Figure 6) and little change in sinuosity of the channels was observed (Figure 6c) other than on the Manohara River, which became more sinuous 1974–2022.

3.3. Flood model outputs

3.3.1. HAND models

The height above the nearest drainage (HAND) derived from the Pleiades DSM displayed good agreement with modelled flood inundation extent from Shrestha et al. (2023) when using the optimum height above channel threshold of 0–4 m (Figure 7). Here, the F1 score and IoU were 0.65 and 0.49 respectively (Figure 8a). The HAND calculation showed
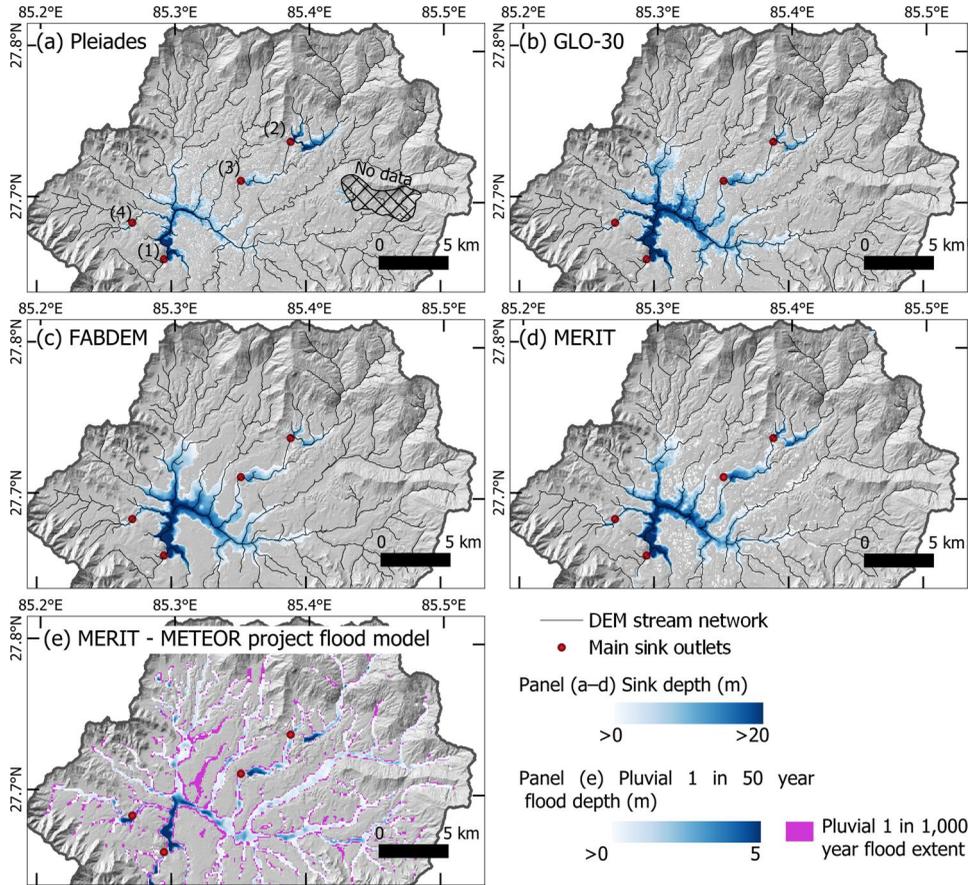
Figure 4. Sinks in each DEM shown (a–d) and 90 m resolution flood model outputs for 1 in 50 and 1,000-year fluvial and pluvial floods (e) (METEOR Project Consortium 2019).

overestimation of flood extent in some built-up areas of the north-west catchment and areas of under prediction including on the Bagmati River (Figure 7). In comparison, the optimum intersection with the high-resolution flood map for the GLO-30 and FABDEM were at HAND thresholds of 3 m (F1 score = 0.59) and 2 m (F1 score = 0.53) respectively (Figure 8).

3.3.2. METEOR models

Comparing the 90 m resolution METEOR and 10 m resolution Shrestha et al. (2023) flood hazard maps revealed poorer agreement. Notably, the 1 in 50 to 1 in 1,000 METEOR hazard maps all showed similar flood extents and therefore similar accuracy scores for all outputs (F1 score between 0.37–0.40) when compared with the Shrestha et al. (2023) model (Figure 9a). The 1 in 50 METEOR hazard map (F1 score = 0.40, IoU = 0.25) displayed closest alignment with the Shrestha et al. (2023) model (Figure 9a, Table 2), nonetheless flood extent was overestimated, particularly around the urbanised core of Kathmandu, although there was closer agreement in the less urbanised sections of the Manohara and Hanumante Rivers (Figure 9b).
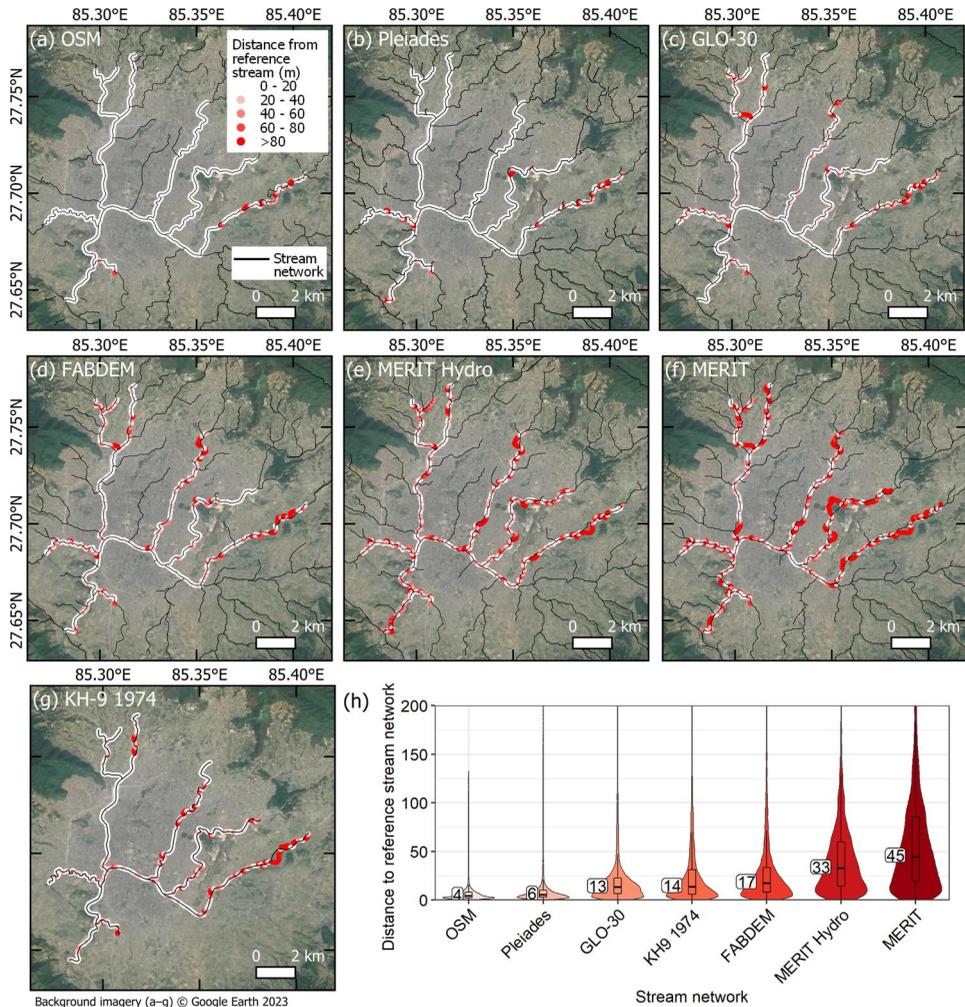
Figure 5. Horizontal offset distance between OpenStreetMap (OSM) (a), DEM-derived (b–f), and KH-9 1974 (g) stream networks compared to a manually digitised reference stream network (show by the extent of the filled points). (h) Violin and boxplots showing the median offset distances for each dataset.

3.3.3. FastFlood model

The FastFlood model run using the same input rainfall as Shrestha et al. (2023) was able to closely reproduce the mapped flood extent for the main river channels (Figure 10). However, some differences were observed in the built-up core of Kathmandu where the FastFlood model included isolated patches of inundation that were not present in the Shrestha et al. (2023) model (Figure 10c). The flood depths between the FastFlood and Shrestha et al. (2023) models also displayed good agreement (Figure 11), with a mean absolute error and root mean square error of 0.46 and 0.76 m respectively.

4. Discussion

4.1. Topographic data

A gap exists between the requirements for high-resolution and up-to-date topographic data to produce robust flood hazard information within urban and topographically
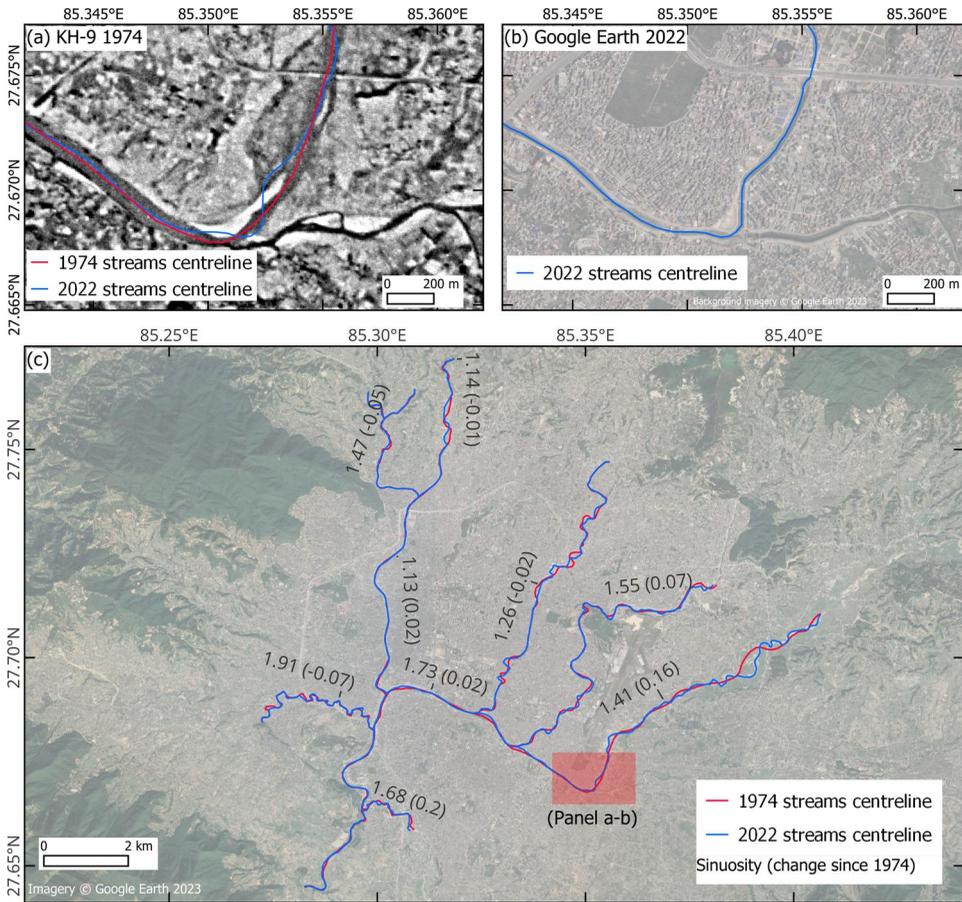
Figure 6. (a) KH-9 1974 orthoimage with streams centreline and 2022 reference stream network overlaid. (b) Google Earth basemap view of the same area in panel (a). (c) Channel sinuosity and change 1974–2022. A positive value indicates an increase in sinuosity.

complex environments, and current open access global DEMs at $\geq$30 m resolution that are a decade or more old (Hawker et al. 2018; Muhadi et al. 2020; Mudashiru et al. 2021). Whilst these open access DEMs can be the basis for robust flood hazard information (Bates et al. 2021), they cannot be assumed to be an adequate representation of the current topography and drainage network.

Sinks were present and spatially coincident in all DEMs evaluated in this study (Figure 4). Identifying these sinks and making appropriate corrections to create a hydrologically conditioned DEM before undertaking flood modelling is common practice (Murphy et al. 2008; Jarihani et al. 2015; Chen et al. 2018). Although, it is important to consider how this hydrological conditioning affects the hydrological response within a catchment (Costabile et al. 2022). However, the spatial association between DEM sinks (Figure 4d) and the METEOR 90 m resolution flood hazard maps (Figure 4e) reveals that the DEM sinks were likely not fully resolved prior to flood map generation. This reflects the site-specific difficulties in creating hydrologically conditioned DEMs in areas of steep or low gradient topography but highlights the importance of this conditioning (Jarihani et al. 2015; Watson et al. 2015).
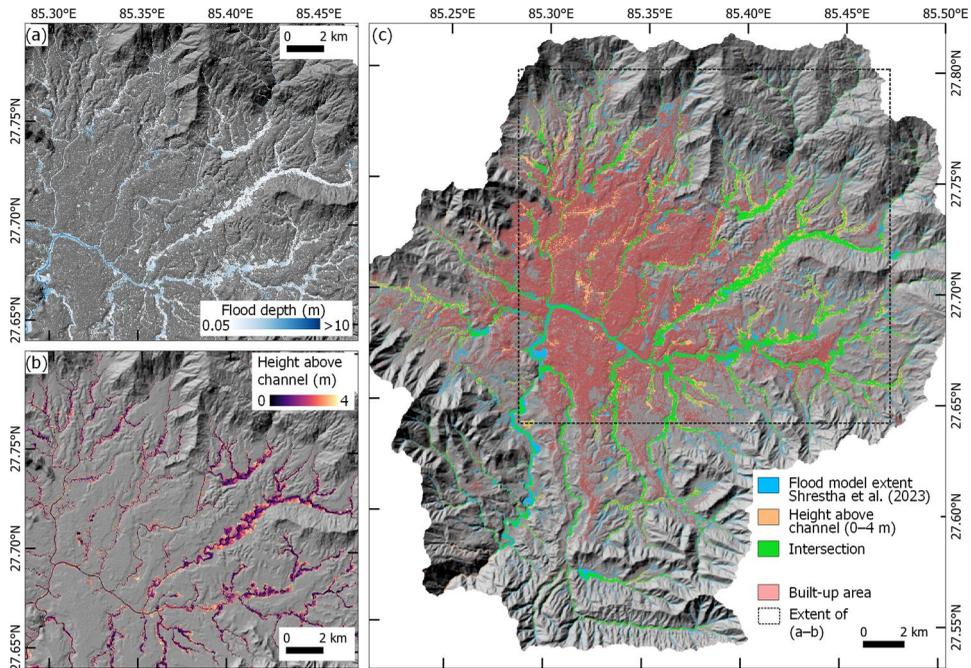
Figure 7. 2D Modelled flood depth from Shrestha et al. (2023) (a), compared to a 0–4 m HAND map (b). (c) Intersection between the flood model and HAND data.
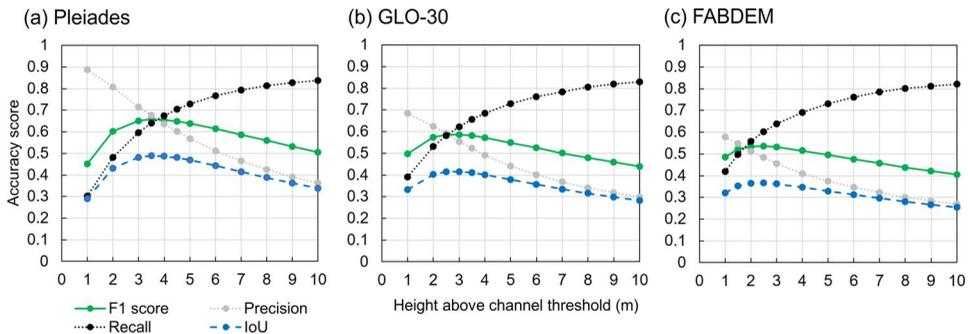
Figure 8. Accuracy scores for the pleiades (a), GLO-30 (b), and FABDEM (c) DEMs when comparing HAND (thresholded at increasing heights above the nearest drainage elevations) and the Shrestha et al. (2023) flood model output.

Application of hydrological corrections to a DEM usually requires a stream channel network to enforce the channel network in the DEM. Traditionally this comprises a 1D centreline, although 2D approaches considering channel width are preferable where the river channel width is smaller than the DEM resolution (Bernard et al. 2022; Costabile et al. 2024). In Kathmandu, the OSM and Pleiades DEM derived stream networks closely matched a reference dataset (4–6 m median horizontal offset), whereas networks derived from the global DEMs had greater deviations (>13 m) (Figure 5). Notably, extreme offsets exceeding 100 m were present in all stream networks (Figure 5h), highlighting local-scale issues in the ability of the DEMs to represent the channel, or channel course changes due to natural meandering and human intervention. In this case, manual inspection of the derived river channel would be required to avoid enforcing an incorrect channel network within a DEM, which would subsequently cause erroneous flow routing.
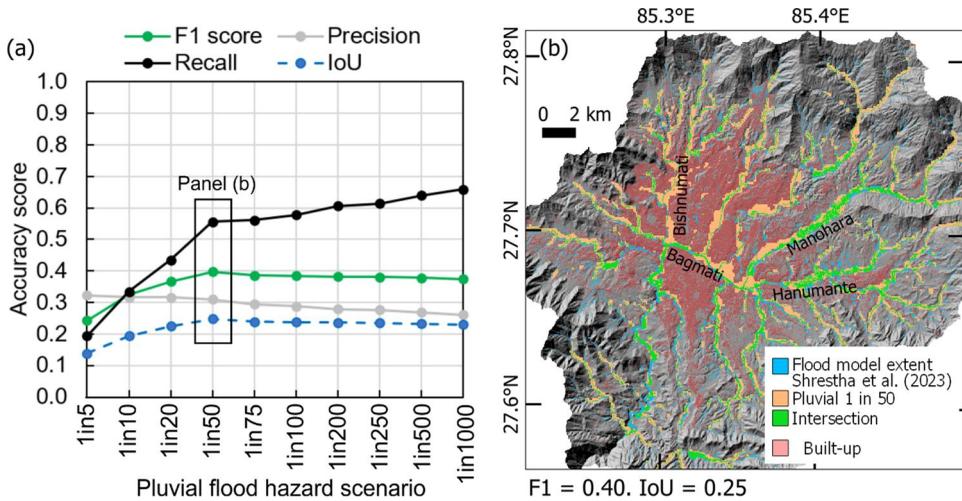
Figure 9. (a) Accuracy scores for the intersection between coarse resolution pluvial flood hazard scenarios and the high-resolution flood hazard model of shreshta et al. (2023). (b) Intersection of the shreshta et al. (2023) flood model maximum extent and the 90 m resolution pluvial 1 in 50 output (METEOR Project Consortium 2019).

4.2. Flood hazard assessment

4.2.1. Global flood hazard models

The 90 m resolution flood hazard maps derived using the Fathom global flood hazard modelling framework (Sampson et al. 2015; Smith et al. 2015), which were published by the METEOR Project Consortium (2019), represented the only open access flood hazard datasets for Kathmandu. However, the pluvial 1 in 50 to 1 in 1,000 hazard maps all showed similar flood extents and low agreement with the 10 m resolution 1 in 100 year mid-future Shrestha et al. (2023) flood model, which has a similar magnitude to a current 1 in 1,000 year event (Figure 9). This primarily appears linked to the location of topographic sinks in different locations in the Kathmandu valley, which accumulated water in the model to create a backwater lake (Figures 4e and 9). Indeed, the quality of the terrain data was regarded as the dominant source of uncertainty in the global flood hazard modelling framework (Sampson et al. 2015). Whilst the METEOR hazard map was not recommended for 'detailed local scale assessments or engineering purposes' (METEOR Project Consortium 2019), it highlights the potential for misinterpretation of the outputs without site-specific knowledge of the topographic constrictions that caused the overestimation of likely flood inundation (Figure 9a,b).

The METEOR 1 in 50 year flood hazard map best matched the reference output of Shrestha et al. (2023); however the mapped inundation extent (77.9 km^2) was 34.5 km^2 greater than that of Shrestha et al. (2023) and only 24.1 km^2 was a true positive classification (Table 2). This would influence the results of studies using these flood maps, such as Mesta et al. (2022) who used the METEOR flood hazard map to quantify the future increase in built-up areas that would occupy flood prone areas. For example, the METEOR 1 in 50 year flood hazard map inundates 18.89 km^2 of the ESA World Cover 2021 built-up area compared to 5.90 km^2 in the reference Shrestha et al. (2023) model (Table 2).

4.2.2. HAND models

In comparison to the METEOR outputs, applying the HAND methodology to the high-resolution Pleaides DEM or global GLO-30 and FABDEMs produced closer agreement

Table 2. Summary of flood model outputs for each model with the closest agreement with Shrestha et al. (2023).

Model	Mapped inundation extent (km²)	True positive	False positive	False negative	F1 score	Intersection over union (IoU)	Inundated ESA World Cover Built up 2020 (km²)
Shrestha et al. (2023)	43.4*	–	–	–	–	–	5.9
HAND 4 m – Pleaides	46.1	29.3	16.8	14.1	0.65	0.5	7.5
HAND 2.5 m – GLO30	42.6	25.2	17.3	18.2	0.59	0.4	11.6
HAND 2 m – FABDEM	54.0	26.1	27.9	17.3	0.54	0.4	15.0
METEOR Fathom Global 1 in 50 years	77.9	24.1	53.8	19.3	0.40	0.3	18.9
FastFlood	36.6	31.5	5.1	11.9	0.79	0.7	5.5

*Clipped to our study area from the original 53 km² in Shrestha et al. (2023).

with the Shrestha et al. (2023) flood model. Here, F1 scores were 0.53 for the FABDEM and 0.66 for the Pleiades DEM, compared to 0.40 for the 1 in 50 year METEOR Fathom Global flood model (F1 = 0.40) (Table 2). Therefore, suggesting that the HAND approach provides a reasonable indication of flood susceptibility that is computationally fast to derive (on the order of minutes). The full HAND workflow including hydro conditioning the input DEM and deriving the stream network does not take more than several hours. However, optimising the HAND outputs requires knowledge of the appropriate height above channel threshold which varied for each DEM (Figure 8) and would vary spatially across the catchment. Nonetheless, the HAND concept of relative elevation above the channel (Figure 1d) is easy to communicate and could therefore be well-suited to local-scale community flood mapping exercises.

The spatial association between HAND derived from a 10 m DEM and the high-resolution Shrestha et al. (2023) flood hazard map (Figure 7) demonstrates that the method is potentially useful to indicate city-scale flood susceptibility in response to fluvial flooding. It could therefore form the basis for initial discussions with communities and policy makers, or be used to estimate flood extent in response to a known water level height from a gauging station. For example, HAND datasets were coupled to the NOAA National Water Model (NWM) to generate rapid flood extent predictions using known water levels (Maidment 2017; Liu et al. 2018; Wing et al. 2019). However, since catchment size, stream order, and flow information are not considered, overestimations of flood extent are apparent in the HAND data where smaller tributaries were included as flood zones, particularly in the central built-up areas of Kathmandu (Figure 7b). Nonetheless, refinements on a channel reach-scale basis are ideally suited to a community engagement project. It is important to note that the HAND outputs are only an indication of flood susceptibility without considering the return period probability of a particular flood magnitude or the dynamic nature of flood water flows. Additionally, with increasing availability of high-resolution DEMs, 2D consideration of river channel and flood plain connectivity can be captured using hydro-geomorphic metrics that offer greater insights into flow routing where channels are wider than the DEM resolution (Bernard et al. 2022; Costabile et al. 2024).

4.2.3. FastFlood model

The FastFlood model is a new, computationally fast way to produce flood hazards maps that is easy to deploy through a web browser interface that uses the local computing resources (van den Bout et al. 2023). When tested in our study using the same input rainfall as Shrestha et al. (2023), it was able to closely reproduce the mapped flood extent
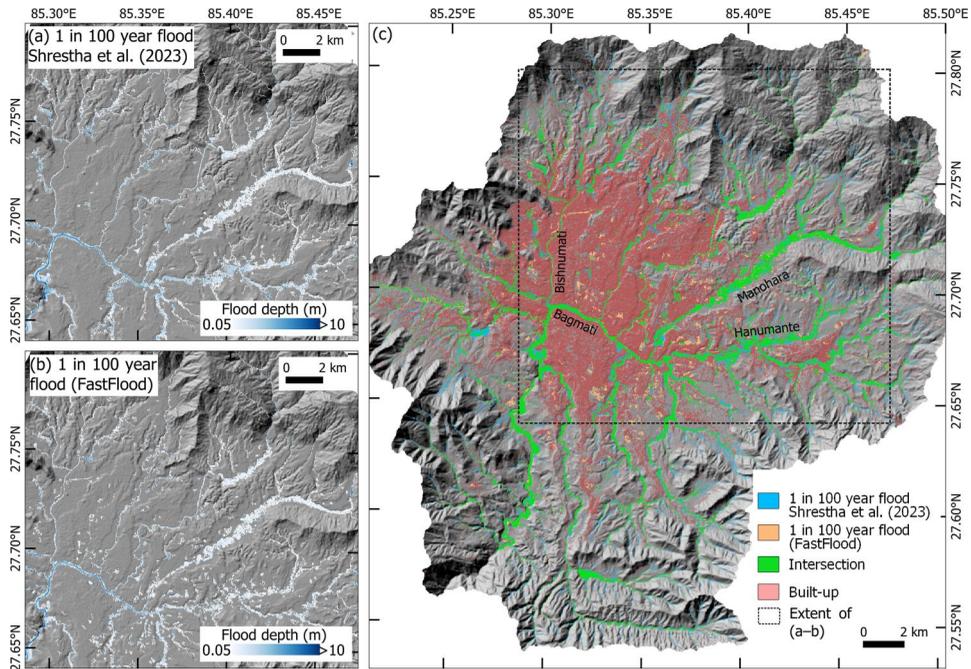
Figure 10. Comparison of 1 in 100-year flood model outputs from Shrestha et al. (2023) and a FastFlood model. (a–b) Example water depths and inundation extent. (c) Intersection between the two model outputs.
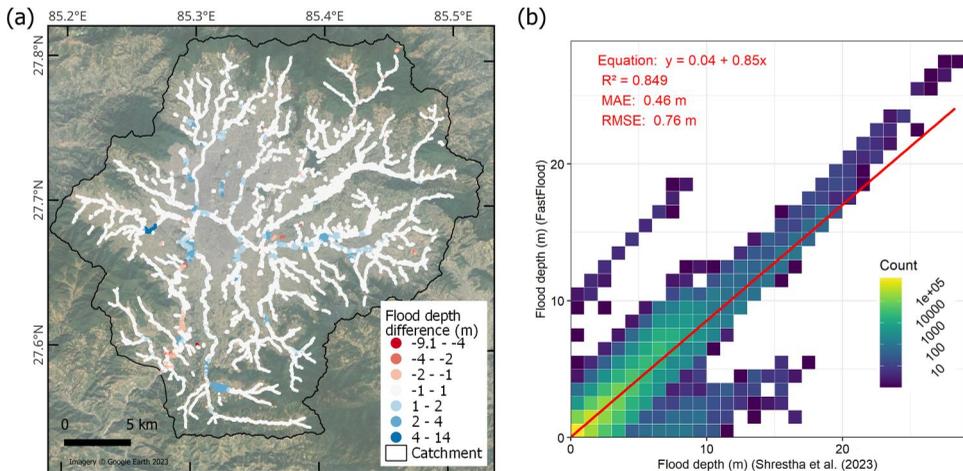
Figure 11. Spatial (a) and graphical (b) representation of the flood depth difference between Shrestha et al. (2023) and the FastFlood model.

across Kathmandu (Figure 10) (F1 = 0.79), and similarly leading to a built up area inundation of 5.45 km^2, compared to 5.90 km^2 from the Shrestha et al. (2023) model (Table 2). However, some differences were observed in the built-up core of Kathmandu where the FastFlood model included isolated patches of inundation, likely where water accumulated in depressions, that were not present in the Shrestha et al. (2023) model (Figure 10c). The difference in flood depths between the FastFlood and Shrestha et al. (2023) models also displayed good agreement (Figure 11), with a mean absolute error and root mean square

error of 0.46 and 0.76 m respectively, which is on the order of uncertainty in the underlying DEM and modelling uncertainty in Shrestha et al. (2023). The FastFlood model uses local computing resources once the inputs are loaded through the website interface and the model we produced (Figure 10) took approximately 15 min to run on a laptop on a DEM with 9.5 million cells, which compares to the 52 h for the Shrestha et al. (2023), which was run using the high-performance computing optimised Hail-Caesar flood model. The FastFlood model was therefore well suited to high-resolution flood hazard modelling across Kathmandu (653 km^2 in our study).

4.3. Outlook

Application of coarse-resolution flood models in urban environments will necessarily persist until high-resolution topographic data become available at low or no cost, and hydraulic modelling computational demands decrease. However, outputs from the FastFlood model demonstrate that robust high-resolution flood hazard modelling at city-scales is now achievable without specialist computing resources. This is particularly valuable for projects such as the Tomorrow's Cities Decision Support Environment (TCDSE) where hazard maps are used to inform community visioning of future risk-sensitive land use plans (Galasso et al. 2021; Jenkins et al. 2022). FastFlood creates new opportunities in this process to iterate multiple flood hazard maps following modification to land cover, building layouts, flood mitigation measures, or topography, to reduce flood risk and optimise decision making.

Conclusion

In this study, we compared published flood hazard maps and new models derived for Kathmandu by evaluating input topography and inundation extents. We demonstrated the importance of DEM choice and hydrological conditioning to mitigate artefacts in the output flood models. Here, all DEMs including a bespoke 10 m resolution DEM and global open access DEMs, featured spatially correlated topographic sinks with depths exceeding 20 m that required pre-processing to allow correct flow routing. It appeared that these sinks were not fully corrected in the only open access flood hazard map available for Kathmandu, which caused an overestimation of flood extent and subsequently showed limited agreement (F1 score = 0.40) with the recently published high-resolution flood hazard map of Shrestha et al. (2023). Instead, we found that a computationally simple height above nearest drainage (HAND) method was better able to replicate the higher resolution flood map if an appropriate depth threshold was selected, and therefore can indicate flood susceptibility using only topographic information. We also demonstrated that the computationally efficient FastFlood model (van den Bout et al. 2023) was best able to match the high-resolution flood model extent (F1 score = 0.79) and water depths (mean absolute error and root mean square error of 0.46 and 0.76 m respectively). This model ran over 200 times faster for the 653 km^2 catchment than the Shrestha et al. (2023) model, which itself used the high-performance computing optimised Hail-Caesar model. The results of this study support the communication of uncertainties and integration of flood hazard information into urban planning frameworks such as the Tomorrow's Cities Decision Support Environment (TCDSE).

Data availability statement

The flood model outputs of this study and supporting data are available at: https://zenodo.org/doi/10.5281/zenodo.11171614

References

Airbus Defence and Space GmbH. 2020. Copernicus DEM -Copernicus digital elevation model product handbook. [accessed 2022 Dec 16]. https://object.cloud.sdsc.edu/v1/AUTH_opentopography/www/metadata/Copernicus_metadata.pdf.

Bates PD, Quinn N, Sampson C, Smith A, Wing O, Sosa J, Savage J, Olcese G, Neal J, Schumann G, et al. 2021. Combined modeling of US fluvial, pluvial, and coastal flood hazard under current and future climates. Water Resou Res. 57(2):e2020WR028673. doi: 10.1029/2020WR028673.

Bernard TG, Davy P, Lague D. 2022. Hydro-geomorphic metrics for high resolution fluvial landscape analysis. JGR Earth Surface. 127(3):e2021JF006535. doi: 10.1029/2021JF006535.

Bourke M, Wilkinson ME, Srdjevic Z. 2022. Nature-based solutions for flow reduction in catchment headwaters. In Spatial flood risk management. Cheltenham, Gloucestershire, United Kingdom: Edward Elgar Publishing.

Chen H, Liang Q, Liu Y, Xie S. 2018. Hydraulic correction method (HCM) to enhance the efficiency of SRTM DEM in flood modeling. J Hydrol. 559:56–70. doi: 10.1016/j.jhydrol.2018.01.056.

Costabile P, Costanzo C, Gandolfi C, Gangi F, Masseroni D. 2022. Effects of DEM depression filling on river drainage patterns and surface runoff generated by 2D rain-on-grid scenarios. Water. 14(7):997. doi: 10.3390/w14070997.

Costabile P, Costanzo C, Lombardo M, Shavers E, Stanislawski LV. 2024. Unravelling spatial heterogeneity of inundation pattern domains for 2D analysis of fluvial landscapes and drainage networks. Journal of Hydrology. 632:130728. doi: 10.1016/j.jhydrol.2024.130728.

Coulthard TJ, Neal JC, Bates PD, Ramirez J, de Almeida GAM, Hancock GR. 2013. Integrating the LISFLOOD-FP 2D hydrodynamic model with the CAESAR model: implications for modelling landscape evolution. Earth Surf Processes Landf. 38(15):1897–1906. doi: 10.1002/esp.3478.

Dehecq A, Gardner AS, Alexandrov O, McMichael S, Hugonnet R, Shean D, Marty M. 2020. Automated processing of declassified KH-9 hexagon satellite images for global elevation change analysis since the 1970s. Front Earth Sci. 8(516):1–21. doi: 10.3389/feart.2020.566802.

Di Baldassarre G, Kooy M, Kemerink JS, Brandimarte L. 2013. Towards understanding the dynamic behaviour of floodplains as human-water systems. Hydrol Earth Syst Sci. 17(8):3235–3244. doi: 10.5194/hess-17-3235-2013.

Farooq M, Shafique M, Khattak MS. 2019. Flood hazard assessment and mapping of River Swat using HEC-RAS 2D model and high-resolution 12-m TanDEM-X DEM (WorldDEM). Nat Hazards. 97(2):477–492. doi: 10.1007/s11069-019-03638-9.

Farr TG, Rosen PA, Caro E, Crippen R, Duren R, Hensley S, Kobrick M, Paller M, Rodriguez E, Roth L, et al. 2007. The shuttle radar topography mission. Rev Geophys. 45(2):1–33. doi: 10.1029/2005RG000183.

Fewtrell TJ, Bates PD, Horritt M, Hunter NM. 2008. Evaluating the effect of scale in flood inundation modelling in urban environments. Hydrol Proces. 22(26):5107–5118. doi: 10.1002/hyp.7148.

Galasso C, McCloskey J, Pelling M, Hope M, Bean CJ, Cremen G, Guragain R, Hancilar U, Menoscal J, Mwang'a K, et al. 2021. Editorial. Risk-based, pro-poor urban design and planning for tomorrow's cities. Int J Disaster Risk Reduct. 58:102158. doi: 10.1016/j.ijdrr.2021.102158.

Hawker L, Bates P, Neal J, Rougier J. 2018. Perspectives on digital elevation model (DEM) simulation for flood modeling in the absence of a high-accuracy open access global DEM. Front Earth Sci. 6:1–9. doi: 10.3389/feart.2018.00233.

Hawker L, Uhe P, Paulo L, Sosa J, Savage J, Sampson C, Neal J. 2022. A 30 m global map of elevation with forests and buildings removed. Environ Res Lett. 17(2):024016. doi: 10.1088/1748-9326/ac4d4f.

Hewett CJM, Wilkinson ME, Jonczyk J, Quinn PF. 2020. Catchment systems engineering: an holistic approach to catchment management. WIREs Water. 7(3):e1417. doi: 10.1002/wat2.1417.

Hoegh-Guldberg O, Jacob D, Taylor M, Bindi M, Brown S, Camilloni I, Diedhiou A, Djalante R, Ebi K, Engelbrecht F, et al. 2018. Impacts of 1.5°C global warming on natural and human systems. In Masson-Delmotte V, Zhai P, Pörtner HO, Roberts D, Skea J, Shukla PR, Pirani A, Moufouma-Okia W, Péan C, Pidcock R, et al., editors. Global warming of 1.5°C. An IPCC special report on the impacts of global warming of 1.5°C above pre-industrial levels and related global greenhouse gas emission pathways, in the context of strengthening the global response to the threat of climate change. Geneva, Switzerland: World Meteorological Organization Technical Document; p. 175–311.

Höhle J, Höhle M. 2009. Accuracy assessment of digital elevation models by means of robust statistical methods. ISPRS J Photogram Rem Sens. 64(4):398–406. doi: 10.1016/j.isprsjprs.2009.02.003.

Ishtiaque A, Shrestha M, Chhetri N. 2017. Rapid urban growth in the kathmandu valley, nepal: monitoring land use land cover dynamics of a himalayan city with landsat imageries. Environments. 4(4):72. doi: 10.3390/environments4040072.

Jarihani AA, Callow JN, McVicar TR, Van Niel TG, Larsen JR. 2015. Satellite-derived digital elevation model (DEM) selection, preparation and correction for hydrodynamic modelling in large, low-gradient and data-sparse catchments. J Hydrol. 524:489–506. doi: 10.1016/j.jhydrol.2015.02.049.

Jenkins LT, Creed MJ, Tarbali K, Muthusamy M, Trogrlić RŠ, Phillips J, Watson CS, Sinclair HD, Galasso C, McCloskey J. 2022. Physics-based simulations of multiple natural hazards for risk-sensitive planning and decision making in expanding urban regions. Int J Disaster Risk Reduct. 84:103338. doi: 10.1016/j.ijdrr.2022.103338.

Jiang A-L, Hsu K, Sanders BF, Sorooshian S. 2023. Topographic hydro-conditioning to resolve surface depression storage and ponding in a fully distributed hydrologic model. Adv Water Resour. 176:104449. doi: 10.1016/j.advwatres.2023.104449.

Johnson JM, Munasinghe D, Eyelade D, Cohen S. 2019. An integrated evaluation of the National Water Model (NWM)–Height Above Nearest Drainage (HAND) flood mapping methodology. Nat Hazards Earth Syst Sci. 19(11):2405–2420. doi: 10.5194/nhess-19-2405-2019.

Kabir S, Patidar S, Xia X, Liang Q, Neal J, Pender G. 2020. A deep convolutional neural network model for rapid prediction of fluvial flood inundation. J Hydrol. 590:125481. doi: 10.1016/j.jhydrol.2020.125481.

Kc S, Shrestha S, Ninsawat S, Chonwattana S. 2021. Predicting flood events in Kathmandu Metropolitan City under climate change and urbanisation. J Environ Manage. 281:111894. doi: 10.1016/j.jenvman.2020.111894.

Kim H, Lee D-K, Sung S. 2016. Effect of urban green spaces and flooded area type on flooding probability. Sustainability. 8(2):134. doi: 10.3390/su8020134.

Lidberg W, Nilsson M, Lundmark T, Ågren AM. 2017. Evaluating preprocessing methods of digital elevation models for hydrological modelling. Hydrol Proces. 31(26):4660–4668. doi: 10.1002/hyp.11385.

Lindsay J. 2014. The whitebox geospatial analysis tools project and open-access GIS.

Lindsay JB. 2016. Whitebox GAT: a case study in geomorphometric analysis. Comput Geosci. 95:75–84. doi: 10.1016/j.cageo.2016.07.003.

Liu YY, Maidment DR, Tarboton DG, Zheng X, Wang S. 2018. A CyberGIS integration and computation framework for high-resolution continental-scale flood inundation mapping. J Am Water Resour Assoc. 54(4):770–784. doi: 10.1111/1752-1688.12660.

Maidment DR. 2017. Conceptual framework for the national flood interoperability experiment. J Am Water Resour Assoc. 53(2):245–257. doi: 10.1111/1752-1688.12474.

Marconcini M, Metz-Marconcini A, Esch T, Gorelick N. 2021. Understanding current trends in global urbanisation-the world settlement footprint suite. giforum. 1:33–38. doi: 10.1553/giscience2021_01_s33.

Martz LW, Garbrecht J. 1992. Numerical definition of drainage network and subcatchment areas from digital elevation models. Comput Geosci. 18(6):747–761. doi: 10.1016/0098-3004(92)90007-E.

McGrath H, Bourgon J-F, Proulx-Bourque J-S, Nastev M, Abo El Ezz A. 2018. A comparison of simplified conceptual models for rapid web-based flood inundation mapping. Nat Hazards. 93(2):905–920. doi: 10.1007/s11069-018-3331-y.

Merz B, Aerts J, Arnbjerg-Nielsen K, Baldi M, Becker A, Bichet A, Blöschl G, Bouwer LM, Brauer A, Cioffi F, et al. 2014. Floods and climate: emerging perspectives for flood risk assessment and management. Nat Hazards Earth Syst Sci. 14(7):1921–1942. doi: 10.5194/nhess-14-1921-2014.

Mesta C, Cremen G, Galasso C. 2022. Urban growth modelling and social vulnerability assessment for a hazardous Kathmandu Valley. Sci Rep. 12(1):6152. doi: 10.1038/s41598-022-09347-x.

METEOR Project Consortium. 2019. Nepal flood maps: fluvial defended, undefended and pluvial for various return periods [online]. [accessed 2023 Jan 16]. https://maps.meteor-project.org/map/flood-npl/#13/27.6489/85.3110.

Min S-K, Zhang X, Zwiers FW, Hegerl GC. 2011. Human contribution to more-intense precipitation extremes. Nature. 470(7334):378–381. doi: 10.1038/nature09763.

Mudashiru RB, Sabtu N, Abustan I, Balogun W. 2021. Flood hazard mapping methods: a review. J Hydrol. 603:126846. doi: 10.1016/j.jhydrol.2021.126846.

Muhadi NA, Abdullah AF, Bejo SK, Mahadi MR, Mijic A. 2020. The use of LiDAR-derived DEM in flood applications: a review. Rem Sens. 12(14):2308. doi: 10.3390/rs12142308.

Murphy PNC, Ogilvie J, Meng F-R, Arp P. 2008. Stream network modelling using lidar and photogrammetric digital elevation models: a comparison and field verification. Hydrol Processes. 22(12):1747–1754. doi: 10.1002/hyp.6770.

Mustafa A, Bruwier M, Archambeau P, Erpicum S, Pirotton M, Dewals B, Teller J. 2018. Effects of spatial planning on future flood risks in urban environments. J Environ Manage. 225:193–204. doi: 10.1016/j.jenvman.2018.07.090.

Muthusamy M, Rivas Casado M, Butler D, Leinster P. 2021. Understanding the effects of digital elevation model resolution in urban fluvial flood modelling. J Hydrol. 596:126088. doi: 10.1016/j.jhydrol.2021.126088.

Neal J, Villanueva I, Wright N, Willis T, Fewtrell T, Bates P. 2012. How much physical complexity is needed to model flood inundation? Hydrol Proces. 26(15):2264–2282. doi: 10.1002/hyp.8339.

Nobre AD, Cuartas LA, Hodnett M, Rennó CD, Rodrigues G, Silveira A, Waterloo M, Saleska S. 2011. Height above the nearest drainage – a hydrologically relevant new terrain model. J Hydrol. 404(1-2):13–29. doi: 10.1016/j.jhydrol.2011.03.051.

Nuth C, Kääb A. 2011. Co-registration and bias corrections of satellite elevation data sets for quantifying glacier thickness change. Cryosphere. 5(1):271–290. doi: 10.1016/10.5194/tc-5-271-2011.

Nyberg B, Buckley SJ, Howell JA, Nanson RA. 2015. Geometric attribute and shape characterization of modern depositional elements: a quantitative GIS method for empirical analysis. Comput. Geosci. 82:191–204. doi: 10.1016/j.cageo.2015.06.003.

OpenStreetMap Contributors. 2022. OpenStreetMap. [online]. [accessed 2022 Nov 17]. https://www.openstreetmap.org

Pelling M. 1999. The political ecology of flood hazard in urban Guyana. Geoforum. 30(3):249–261. doi: 10.1016/S0016-7185(99)00015-9.

Pradhan-Salike I, Raj Pokharel J. 2017. Impact of urbanization and climate change on urban flooding: a case of the Kathmandu valley. J Nat Resour Dev. 7:56–66. doi: 10.5027/jnrd.v7i0.07.

Reckien D, Creutzig F, Fernandez B, Lwasa S, Tovar-Restrepo M, Mcevoy D, Satterthwaite D. 2017. Climate change, equity and the sustainable development goals: an urban perspective. Environ Urbaniz. 29(1):159–182. doi: 10.1177/0956247816677778.

Rennó CD, Nobre AD, Cuartas LA, Soares JV, Hodnett MG, Tomasella J, Waterloo MJ. 2008. HAND, a new terrain descriptor using SRTM-DEM: mapping terra-firme rainforest environments in Amazonia. Remote Sens Environ. 112(9):3469–3481. doi: 10.1016/j.rse.2008.03.018.

Reuter HI, Hengl T, Gessler P, Soille P. 2009. Chapter 4 preparation of DEMs for geomorphometric analysis. In: Hengl T, Reuter HI, editors. Developments in soil science. Amsterdam, Netherlands: Elsevier; p. 87–120.

Rincón D, Khan UT, Armenakis C. 2018. Flood risk mapping using GIS and multi-criteria analysis: a greater toronto area case study. Geosciences. 8(8):275. doi: 10.3390/geosciences8080275.

Saksena S, Merwade V. 2015. Incorporating the effect of DEM resolution and accuracy for improved flood inundation mapping. J Hydrol. 530:180–194. doi: 10.1016/j.jhydrol.2015.09.069.

Sampson CC, Smith AM, Bates PD, Neal JC, Alfieri L, Freer JE. 2015. A high-resolution global flood hazard model. Water Resour Res. 51(9):7358–7381. doi: 10.1002/2015WR016954.

Sampson CC, Smith AM, Bates PD, Neal JC, Trigg MA. 2016. Perspectives on open access high resolution digital elevation models to produce global flood hazard layers. Front Earth Sci. 3:1–6. doi: 10.3389/feart.2015.00085.

Saunders W. 2000. Preparation of DEMs for use in environmental modeling analysis. Hydrologic and hydraulic modeling support. Redlands, CA: ESRI; p. 29–51.

Sevara C. 2013. Top secret topographies: recovering two and three-dimensional archaeological information from historic reconnaissance datasets using image-based modelling techniques. Int J Herit Digital Era. 2(3):395–418. doi: 10.1260/2047-4970.2.3.395.

Shean DE, Alexandrov O, Moratto ZM, Smith BE, Joughin IR, Porter C, Morin P. 2016. An automated, open-source pipeline for mass production of digital elevation models (DEMs) from very-high-resolution commercial stereo satellite imagery. ISPRS J Photogram Rem Sens. 116:101–117. doi: 10.1016/j.isprsjprs.2016.03.012.

Shrestha D, Basnyat DB, Gyawali J, Creed MJ, Sinclair HD, Golding B, Muthusamy M, Shrestha S, Watson CS, Subedi DL, et al. 2023. Rainfall extremes under future climate change with implications for urban flood risk in Kathmandu, Nepal. Int J Dis Risk Reduct. 97:103997. doi: 10.1016/j.ijdrr.2023.103997.

Smith A, Sampson C, Bates P. 2015. Regional flood frequency analysis at the global scale. Water Resour Res. 51(1):539–553. doi: 10.1002/2014WR015814.

Smith MW, Carrivick JL, Quincey DJ. 2015. Structure from motion photogrammetry in physical geography. Progr Phys Geogr. 40(2):1–29. doi: 10.1016/10.1177/0309133315615805.

Tufano R, Guerriero L, Annibali Corona M, Cianflone G, Di Martire D, Ietto F, Novellino A, Rispoli C, Zito C, Calcaterra D. 2023. Multiscenario flood hazard assessment using probabilistic runoff hydrograph estimation and 2D hydrodynamic modelling. Nat Hazards. 116(1):1029–1051. doi: 10.1007/s11069-022-05710-3.

van den Bout B, Jetten VG, van Westen CJ, Lombardo L. 2023. A breakthrough in fast flood simulation. Environ Model Soft. 168:105787. doi: 10.1016/j.envsoft.2023.105787.

Vollmer D, Grêt-Regamey A. 2013. Rivers as municipal infrastructure: demand for environmental services in informal settlements along an Indonesian river. Global Environ. Change. 23(6):1542–1555. doi: 10.1016/j.gloenvcha.2013.10.001.

Watson CS, Carrivick J, Quincey D. 2015. An improved method to represent DEM uncertainty in glacial lake outburst flood propagation using stochastic simulations. J Hydrol. 529(Part 3):1373–1389. doi: 10.1016/j.jhydrol.2015.08.046.

Webber MK, Samaras C. 2022. A review of decision making under deep uncertainty applications using green infrastructure for flood management. Earth's Fut. 10(7):e2021EF002322. doi: 10.1029/2021EF002322.

Wechsler SP. 2007. Uncertainties associated with digital elevation models for hydrologic applications: a review. Hydrol Earth Syst Sci. 11(4):1481–1500. doi: 10.5194/hess-11-1481-2007.

Wheater H, Evans E. 2009. Land use, water management and future flood risk. Land Use Policy. 26:s251–S264. doi: 10.1016/j.landusepol.2009.08.019.

Wing OEJ, Bates PD, Sampson CC, Smith AM, Johnson KA, Erickson TA. 2017. Validation of a 30 m resolution flood hazard model of the conterminous United States. Water Resour Res. 53(9):7968–7986. doi: 10.1002/2017WR020917.

Wing OEJ, Sampson CC, Bates PD, Quinn N, Smith AM, Neal JC. 2019. A flood inundation forecast of Hurricane Harvey using a continental-scale 2D hydrodynamic model. J Hydrol. 4:100039. doi: 10.1016/j.hydroa.2019.100039.

Xing Y, Liang Q, Wang G, Ming X, Xia X. 2019. City-scale hydrodynamic modelling of urban flash floods: the issues of scale and resolution. Nat Hazards. 96(1):473–496. doi: 10.1007/s11069-018-3553-z.

Yalcin E. 2020. Assessing the impact of topography and land cover data resolutions on two-dimensional HEC-RAS hydrodynamic model simulations for urban flood hazard analysis. Nat Hazards. 101(3):995–1017. doi: 10.1007/s11069-020-03906-z.

Yamazaki D, Ikeshima D, Sosa J, Bates PD, Allen GH, Pavelsky TM. 2019. MERIT Hydro: A high-resolution global hydrography map based on latest topography dataset. Water Resou Res. 55(6):5053–5073. doi: 10.1029/2019WR024873.

Yamazaki D, Ikeshima D, Tawatari R, Yamaguchi T, O'Loughlin F, Neal JC, Sampson CC, Kanae S, Bates PD. 2017. A high-accuracy map of global terrain elevations. Geophys Res Lett. 44(11):5844–5853. doi: 10.1002/2017GL072874.

Zanaga D, Van De Kerchove R, Daems D, De Keersmaecker W, Brockmann C, Kirches G, Wevers J, Cartus O, Santoro M, Fritz S. 2022. ESA WorldCover 10 m 2021 v200.